Cite this as:
Lucyna Grządziel, Maciej Krzywiecki, Georgi Genchev, Andreas Erbe: Effect of order and disorder on degradation processes of copper phthalocyanine nanolayers. Synthetic Metals, 223, 199-204 (2017). DOI: 10.1016/j.synthmet.2016.11.024

Final copy-edited version of the manuscript is available from:
https://doi.org/10.1016/j.synthmet.2016.11.024

Effect of order and disorder on degradation processes of copper phthalocyanine nanolayers

Lucyna Grządziel[1], Maciej Krzywiecki[1,2], Georgi Genchev[2], Andreas Erbe[2,3]

[1] *Institute of Physics – Center for Science and Education, Silesian University of Technology, S. Konarskiego Str. 22B, 44-100 Gliwice, Poland*
[2] *Max-Planck-Institut für Eisenforschung GmbH, Max-Planck-Str. 1, 40237 Düsseldorf, Germany*
[3] *Department of Materials Science and Engineering, NTNU, Norwegian University of Science and Technology, 7491 Trondheim, Norway*

Abstract

The impact was examined of surface ordering of 50 nm-thick copper phthalocyanine (CuPc) layers on the layer's susceptibility to ambience-induced degradation processes. The surface morphology of CuPc layers obtained by physical vapor deposition with different deposition rates, 0.01 nm/s (r_1) and 0.02 nm/s (r_2), was diagnosed applying atomic force and scanning electron microscopes. The images exhibited compact, ordered surface topography with crystallites of homogeneous geometry for a layer with r_1 while randomly distributed bigger crystallites on a rougher and more expanded surface for a layer with r_2. X-ray diffraction revealed the α-form of phthalocyanine, mostly with an orientation of the a axis perpendicular to the substrate plane. Mean grain size in bulk was slightly larger for CuPc with r_2. . Energy dispersive X-ray spectroscopy demonstrated an increase of C/Cu and N/Cu elemental ratios compared to the expected composition for both layers but significantly more pronounced for layer with r_2. Morphological features and traces of CuPc-air interaction were mirrored also in the Raman spectra. Samples with r_2 exhibited an increased peak width, and their peaks were shifted compared to samples with r_1, which was attributed to surface disorder. The Raman spectra exhibited the appearance of additional peaks of oxidation products indicating C-O-C, C=O and N-O bonds, with intensities coinciding to an increased carbon and nitrogen content. More intensive peaks were recorded for layers obtained with higher deposition rate, proving their stronger susceptibility to environment-induced degradation processes.

Keywords
nanoelectronics, organic thin film, phthalocyanine, degradation processes, morphology, Raman spectroscopy

---

* Corresponding author, tel.: +48 (32) 237 20 01; fax: +48 (32) 237 22 16
E-mail: Lucyna.Grzadziel@polsl.pl

Introduction

Promising candidates for several electronic applications emerge from the group of organic semiconductors, the metallophthalocyanines (MePc) – heterocyclic conjugated molecules with high thermal and chemical stability [1]. In the form of thin films, MePc's have been already tested in third generation solar cells, gas sensors and advanced opto-electronics technologies [2,3,4,5,6,7].

However, operating in a "real world" environment, the organic-based devices are inevitably subjected to the influence of the ambient conditions [8]. Particularly, exposure to surrounding air leads to the adsorption of species on the surface of organic layer. Adsorption may be accompanied by charge transfer and subsequently provoke changes of surface chemical structure, electronic and vibrational properties [9]. All air-originated changes of layer properties degraded the device efficiency, lifetime and consequently have an impact on the effective use of devices [10].

Yet, the aging of phthalocyanines and the other organic thin films was mainly investigated by means of the electrical measurements [11,12,13], Kelvin probe [12], and photoemission methods like e.g. photoemission yield spectroscopy [14], ultraviolet and X-Ray photoelectron spectroscopies (XPS) [15]. In these studies, the main emphasis was placed on specification of the variation of electronic and chemical properties after interaction with air over different time scales [16]. For instance, the propensity of organic layers for a strong interaction with the atmosphere depends on their morphological features, which in turn are determined during film preparation by specific conditions [17].

In this work, the products of air-induced chemical degradation of 50 nm-thick copper phthalocyanine (CuPc) films on Si(111) was investigated by energy dispersive X-ray (EDX) and Raman spectroscopy, in relation to the surface topographical ordering. The variation of surface morphology was obtained during the deposition process by changing the deposition rate. Samples' morphologies were characterized by atomic force and scanning electron microscopies (AFM and SEM, respectively). The phase and mean crystallite size were checked by X-ray diffraction (XRD). The analysis of Raman peak shape and positioning revealed impact of samples' morphological order/disorder. Up to now, Raman spectroscopy as fast, non-destructive and cost-effective diagnostic method [18], has been applied for MePcs mainly as the tool for distinguishing of their molecular orientation and polymorphic phase [19,20,21,22]. At present, the detailed analysis of Raman peaks suggested ability of this technique to fingerprint phthalocyanine surface homogeneity and its inclination for degradation processes.

Experimental details

Sample preparation

CuPc (Copper (II) Phthalocyanine, see Figure 1 for molecule scheme; molecular formula:$C_{32}H_{16}N_8Cu$) layers with thickness of 50 nm were thermally evaporated from sublimed powder (Sigma-Aldrich, >97% purity, β-form) in high vacuum by physical vapor deposition on p-type Si(111) native substrates (BOSCH GmbH) kept at room temperature. The powder was degassed and purified in vacuum conditions at 220°C prior deposition in order to extract residual contaminations. Substrates were pre-cleaned with acetone in an ultrasonic bath, rinsed with deionized water and dried with nitrogen. The CuPc films were deposited at the pressure of 10^{-6} Pa with different deposition rates *r* equal to 0.01 nm/s and 0.02 nm/s. The respective samples will be denoted also as r_1 and r_2 hereafter. The thicknesses of the layers were controlled by a quartz crystal microbalance (Inficon XTC3M) and verified with AFM measurements on the layer edges. The obtained film thickness assured that no substrate/overlayer interfacial effects would affect the studies. After deposition, the CuPc films were subjected to ambient air exposure for a 1-year period at room temperature in a dry box with stable humidity of 40%.

Figure 1

Characterization

The surface morphology of obtained CuPc thin films was investigated by AFM and SEM.

The AFM measurements were performed using a PSIA XE-70 microscope in non-contact mode (NC-AFM) applying BS Tap300Al cantilevers with resonance frequency of 300 kHz and spring constant of 40 Nm^{-1}. Acquired images were processed using image processing software WSxM 5.0® [23] in order to revise sample inclination and distortions caused by the z-scanning stage. All quantitative morphological parameters were specified with the application of WSxM built-in algorithms. As a measure of surface roughness, the root mean square (RMS) of roughness was quantified, where the root mean deviation from a plane was analyzed. Surface area estimation was performed by triangulating the surface (as stated in the algorithm description) and summing up their area to obtain the total area. Further details can be found elsewhere [24].

The SEM images were collected utilizing a Carl Zeiss LEO 1550 VP microscope working with an in lens detector (working distance: 3 mm; ETH voltage: 15 kV).

In order to determine the phase and the mean grain size in bulk of the thin films of the examined samples, grazing incidence X-ray diffraction (GI-XRD) on a Seifert ID 3003 diffractometer (GE Inspection Technologies, Germany) was used, with Co-Kα radiation (0.178897 nm) and a Meteor0D detector. The diffraction patterns have been collected at an angle of incidence $\alpha = 1.0°$ within a range of scattering angle 2ϴ of $5° < 2\Theta < 70°$. Step size was 0.05° and step time 30 s. The X-ray tube was operated at 40 kV and 30 mA.

For elemental chemical analysis of the material, the EDX spectroscopy (Oxford Instruments) was used. The EDX setup was integrated into the SEM installation.

To collect the vibrational data the Raman spectra were recorded using a Horiba Jobin Yvon Labram confocal Raman microscope working in backscattering geometry with a long working distance objective (magnification 50×, numerical aperture 0.5) for sample

illumination and scattered light collection. Excitation source was an Argon ion laser (wavelength 514.342 nm). The spectral acquisition time was 20 s. Raman spectra were analysed by multi-Lorentzian peak fitting using procedures implemented in OriginLab Origin 8.5. All of the uncertainties were calculated with use of standard uncertainty propagation methods [[25]].

Results and discussion

Fig. 2 presents the NC-AFM surface topography images recorded for samples r_1 and r_2 (Fig. 2 a and b respectively). The images are combined with roughness analysis histogram presenting the distribution of grain heights (Fig. 2 c and d).

Fig.2

The images show well-developed phthalocyanine surfaces with grains of different size and orientation, dependent on deposition rate. For r_1 CuPc (Fig. 2 a), an ordered, compact and homogeneous topography with bent crystallites oriented parallel to the substrate plane was observed. For r_2 (Fig. 2 b), the surface topography was characterized by randomly distributed bigger (taller) crystallites standing upright with respect to the substrate plane. Standing grains were accompanied by deeper, more ordered, laying grains of curved shape.

Root mean square roughness was determined as 2.0(2) nm for r_1 and 16.4(2) nm for r_2. The value of average grain height grew from 3.1(2) nm for r_1 to 13.6(2) nm for r_2. The surface area also increased from 1.01(3) μm^2 to 1.22(3) μm^2 for r_1 and r_2 films, respectively. Layers with larger surface area as in this case r_2 obtained by faster deposition are supposed to be more susceptible to active surface processes.

Fig.3

The SEM images for samples r_1 and r_2 shown in Fig. 3 a and b, respectively, visualized similar features of the surface topography like observed by AFM.

Both microscopic investigations confirmed the strong impact of the deposition rate on the CuPc surface morphology, including crystallite ordering.

XRD patterns of both samples were very similar, showing the major peak at the diffraction angle 2Θ close to 8° (Fig. 4). This value corresponds to the α-form of phthalocyanine, as described by Berger et al. [26] for CuPc films deposited at a low sublimation pressure on substrates held at room temperature. No traces of transition to β-form of phthalocyanine polymorph (demanding layer annealing at around 200° [20]) were observed. For the detected peak position, the interplanar distance d was calculated applying the Bragg equation [27]. From the formula [27] $d = \lambda/2\sin\Theta$, where the X-ray wavelength of the Co-Kα source $\lambda = 0.179$ nm, the value of $d = 1.28$ nm was obtained. This value is equal to the half of the unit cell length of the CuPc in direction of the a axis [26]. The result shows the possibility that the CuPc films were formed with the a axis located perpendicular to the substrate plane and the b axis, as stacking axis of phthalocyanine molecules, oriented parallel to the substrate [26]. In consequence, crystallites should be formed with the dominating laying orientation parallel to the substrate's surface. This statement is coinciding well with the microscopic observations. A laying arrangement of crystallites implied a nearly standing geometry of the CuPc molecules with respect to the substrate plane. A scheme depicting molecular arrangement is presented as an inset in Fig. 4. This growth mode with preferential standing molecular orientation, i.e. a lying orientation of the crystallite stacking axis, was observed before for CuPc layers deposited on rough, polycrystalline or ill-defined technical substrates [28,29,30].

Fig. 4

Employing XRD data, the mean crystalline size L in the bulk of CuPc films was estimated. Using the Scherrer formula [27], $L = K_s\lambda/\beta'\cos\Theta$, where K_s is a shape-depended constant ($K_s \sim 0.9$ for MePc materials [24]) and β' the full width at half of maximum (FWHM) of the most intensive peak, L was calculated as close to 26.6(3)nm and 27.5(3) nm for r_1 and r_2 layers, respectively, indicating slight grain enlargement provoked by faster deposition rate.

Despite similarities in volume morphology, differences in CuPc surface topography could have an impact on surface processes, like oxygen or carbon oxides adsorption from surrounding atmosphere [17], or surface oxidation. It is known, that the α-phase of MePc films adsorbs a larger amount of oxygen or oxidizing agents in comparison to the other phases [[31],[32]] and the topography can significantly enhance adsorption.

EDX was utilized to characterize the chemical composition after the samples were exposed to air. Table 1 presents the concentrations of elements C, N, Cu and O as well as Si originating from the substrate for r_1 and r_2 layers.

Table 1

Basing on the EDX results, the O/Cu concentrations ratio was determined as close to 0.8 for both types of CuPc films. Oxygen is not present in CuPc molecules. It is worth pointing out that within the limits of the sensitivity, there was no essential difference in oxygen content between the layers. After our previous XPS studies of chemical composition of an as-deposited 32 nm-CuPc layer [9], where no oxygen signal was detected, we eliminated the preparation process and source impurities as the origin of the detected oxygen. By XPS after air exposure [9], we reported the existence of O-C, O=C and H_2O-originating components of the O 1s peak spectrum, These are the result of interaction between phthalocyanine and surrounding atmosphere. The O concentration almost on the same level as Cu as detected in this study may hence also result from CuPc-air interaction. However, the impact of oxygen from native SiO_2 on the total oxygen level could not be excluded, but supposed contribution of oxide should be balanced for both kinds of samples.

For the C/Cu ratio, significantly different values of ~95 and ~171 were received for r_1 and r_2 samples, respectively. For pure CuPc, the expected C/Cu ratio equals 32 and similar value we previously observed during XPS studies for various as-deposited CuPc layers [[33]]. Increased values show higher concentrations of carbon contaminations. Especially r_2 shows extremely high values of carbon. The elevated relative concentration of carbon coincided well with our previous XPS findings [9], where for comparable in thickness, air-exposed CuPc layers the C-O, C=O additional components of C 1s peak were recognized.

The N/Cu ratio was estimated as ~15 and ~24 for r_1 and r_2, respectively, indicating a substantial nitrogen excess in both cases. The effect was more significant for r_2 samples, comparing to the expected and experimentally confirmed by XPS [33] value of 8 for pure CuPc. Results correlated well with reported appearance of additional N-O components of N 1s peak for air exposed 32 nm-CuPc layer during our previous XPS studies [9]. Almost two times higher uptake of carbon and nitrogen contaminations from the ambient air in the layer deposited with higher r could be related to their more complex surface morphology which means more rough and developed surface area comparing to layer with lower r.

Fig. 5

Raman spectra of air exposed CuPc layers were measured, and are presented in Fig. 5. Generally, both spectra revealed similar spectral features, although differences in details with regard to peak shapes and positioning were observed.

The strong Raman peak around 522 cm^{-1} [34] was assigned to the main Raman active phonon of the silicon substrate. This signal was comparable for both kinds of samples, and does not yield any preparation specific information. It's consistent position does, however, confirm the stability of the spectrometer.

Appearing before Si signal two peaks located close to 232 cm^{-1} and 254 cm^{-1} could be attributed to phthalocyanine-originated Cu-N bond deformation after the statements of Basova et al. [35] and Wang et al. [36]. Further, two intensive peaks situated close to 593 cm^{-1} and 680 cm^{-1} were assigned to CuPc macro-cycle ring breathing mode and C-N-C and N-C-C bending modes, respectively following Beaulieu-Houle et al. [37]. Peaks located at about 833 cm^{-1}, 1037 cm^{-1} and 1141 cm^{-1} originated from C-N stretching, C-H bending and pyrrole breathing vibrational mode, respectively (after Wang et al. [36]). Two other very intensive peaks near 1344 cm^{-1} and 1533 cm^{-1} were also experimentally observed by authors in Ref. [36] and attributed to pyrrole C-N stretching vibration mode and isoindole mode, respectively. Intensities of detected peaks originating from r_2 CuPc layers were doubled with respect to intensities of peaks from r_1 layers what correlated to the enhanced C concentrations.

Fig.6

In current work, the special attention was focused on the spectral region of 1300 - 1500 cm^{-1} [20]. For this spectral window, a detailed analysis was conducted based on a multi-Lorentzian decomposition procedure for asymmetric peaks [20,38] for both types of CuPc layers (shown in Fig. 6 a and b for samples r_1 and r_2, respectively). Table 2 presents data concerning the decomposed peak position, peak width represented by FWHM, and peak assignment following an analysis by Basova et al. [35].

Table 2

Analyzing the Raman peak positions in the selected spectral window, a frequency shift towards lower frequency was observed for peaks from r_2 layers compared to r_1. The average shift was 2.2 cm^{-1}. At the same time, the peaks of r_2 showed an increased FWHM. For r_2 layers, the peaks were on average 1.4 times broader then for r_1.

An analogue effect was observed by Guo et al. [39] for nanocrystals embedded in amorphous silicon ruthenium thin films. The authors of ref. [39] interpreted a peak localization shift and width decrease as results of short-range order improvement during the crystallization process. Moreover, Salvan et al. [38], during the Raman study of thin organic films of 3,4,9,10-perylene tetracarboxylic dianhydride, observed a decrease of bands' FWHM value. The result was related to the structural recovery induced by the growth on a heated substrate during deposition, i.e., to the development of more ordered crystalline domains [38]. Similar studies by Stenzel et al. [40] showed that for CuPcs with incorporated metal clusters (as well as for similar materials like fullerens or perylene derivatives), the complicated geometry of modified layers could cause stress and deformation of surrounding molecules. Stress and deformation lead to statistically distributed vibrational frequency shift, and consequently to an inhomogeneously broadened Raman spectrum.

Following above literature statements, the observed Raman peak shift and increase of peak FWHM value reflect the morphological differences observed between samples r_1 and r_2. Particularly, Raman spectral features' changes pointed to morphological disorder or inhomogeneous geometry of the surface of r_2 CuPc layers, comparing to the more ordered topography of r_1 ones. Bulk geometry was similar for both kinds of samples, as shown above,

and can hence not be responsible for the observed effects. These observations coincide well with microscopic images.

In the Raman spectra, the traces of products of the air-induced degradation processes were also observed for both kinds of CuPc layers. The peak located close to 1100 cm^{-1} could be assigned (after Torres et al. [[41]]) to symmetric stretching of the C-O-C bonds, while a weak feature appeared around 1780 cm^{-1} is originating from a C=O vibration [38]. Intensities of these peaks after background subtraction are approximately two times higher for r_2 CuPcs in comparison to r_1 layers. This higher intensity could be related to elevated concentrations of carbon determined from EDX measurements, affected by the corresponding disordered or ordered surface topography.

Another, most likely air-induced Raman peak was detected close to 1157 cm^{-1} and may be assigned to N-O stretching vibrations following Paulat et al. [[42]]. Peak intensities, again higher for r_2 layers, could correspond to enhanced concentration of nitrogen revealed by EDX.

Appearance of additional C-O-C, C=O and N-O vibrations in phthalocyanines' Raman spectra coincided well with our previous XPS investigations of ambience-related changes in surface chemistry of CuPc layers with similar thickness [9]. In aforementioned studies similar components were recognized [9].

Thus, the more complex and disordered surface morphology of r_2 samples led to their stronger susceptibility for adsorption of substances from the environment, compared to the more uniform, ordered surface of r_1 samples. Hence, the disordered CuPc surface is more vulnerable for air-induced degradation processes. The statements were confirmed by Raman studies allowing to differentiate the samples' morphological ordering and reveal additional vibrations from reaction products.

Summary and conclusions

The 50 nm thick CuPc layers of different surface morphology were subjected to controlled air exposure and then investigated by surface microscopic and diffraction techniques, and with Raman spectroscopy. A variation of surface morphology was obtained during the deposition process by altering the deposition rate.

The surface topography of CuPc layers was compact, with bent crystallites of homogeneous geometry, for layers deposited with lower rate. Layers deposited faster showed bigger crystallites, randomly distributed, causing increased surface roughness, average grain height, and surface area.

Bulk morphological investigations conducted XRD indicated the α-form of phthalocyanine, with the crystallographic a-axis perpendicular to the surface, and the b-axis which corresponds to the stacking direction, parallel to the surface. The mean grain size was slightly larger for CuPc obtained with higher deposition rate.

EDX revealed an enlarged C/Cu and N/Cu ratio for both samples after exposure to air for 1 year. This increase was significantly higher for the faster deposited films. Enhanced concentration of carbon and nitrogen in layers with doubled deposition rate was related to the expanded surface morphology, which is supposed to be more inclined for surface processes.

Morphological features were mirrored in the Raman spectra. An analysis of the peak shift and FWHM of Raman peaks showed that changes of these parameters reflect the CuPc order and disorder. The Raman spectra exhibited additional peaks of the bonds such as C-O-C, C=O, and N-O, which may originate from adsorbed contaminants or from oxidation products. The intensities coincided with an increased carbon and nitrogen content. More intensive peaks related to oxidized species were detected for layers obtained with higher deposition rate, i.e., samples with disordered surface morphology. This observation proves their stronger susceptibility to environment-induced degradation processes.

Acknowledgements

This work was financially supported by the Polish budget for science in years 2013-2015 (by Ministry for Science and Higher Education) within Iuventus Plus IP2012 019072 project through the Silesian University of Technology, Institute of Physics. Authors would like to acknowledge B. Breitbach for support on XRD experiment and E. Müller-Lorenz from Max Planck Institute for Iron Research, Duesseldorf, for support on SEM/EDX measurements.

Figure captions

Figure 1
Scheme of CuPc molecule.

Figure 2
NC-AFM images of surface topography of 50 nm-CuPc layers obtained with deposition rates r_1 (a) and r_2 (b). Corresponding roughness analysis histograms (c) and (d), respectively.

Figure 3
SEM images of surface morphology for r_1 (a) and r_2 (b) CuPc layers.

Figure 4
XRD patterns for r_1 and r_2 CuPc samples in the region of diffraction angle 2Θ of the most prominent CuPc diffraction peak. Inset: Scheme of molecular arrangement.

Figure 5
Survey Raman spectra for r_1 and r_2 50 nm-CuPc layers after air exposure.

Figure 6
Raman spectral windows for r_1 (a) and r_2 (b) 50 nm-CuPc layers with depicted multi-Lorentzian decomposition of asymmetric peaks.

References

1[1] J. Simon, J.-J. Andre, Molecular Semiconductors, Springer, Berlin, 1985.

2[2] O.A. Melville, B. H. Lessard, T.P. Bender, ACS Appl. Mater. Interfaces 7 (2015) 13105.

3[3] Ch.D. Dimitrakopoulos, P.R.L. Malenfant, Adv. Mater. 14 (2002) 99.

4[4] P.-L. Ong, I.A. Levitsky, Energies 3 (2010) 313.

5[5] G. Guillaud, J. Simon, J.P. Germain, Coord. Chem. Rev. 178-180 (1998) 1433.

6[6] A. S. Komolov, E.F. Lazneva, N.B. Gerasimova, M.V. Zimina, P. Si, Yu.A. Panina, Phys. Solid State 57 (2015) 255.

7[7] Y. Gao, Mater. Sci. Eng. R 68 (2010) 39.

8[8] M. Bouvet, Anal. Bioanal. Chem. 384 (2006) 366.

9[9] L. Grządziel, M. Krzywiecki, Synt. Met. 210 (2015) 141.

10[10] J.C. Bernede, J. Chil. Chem. Soc. 53 (2008) 1549.

11[11] A. de Haan, M. Debliquy, A. Decroly, Sens. Actuator B-Chem. 57 (1999) 69.

12[12] Y. Harima, K. Yamashita, H. Ishii, K. Seki, Thin Solid Films 366 (2000) 237.

13[13] J. Brunet, A. Pauly, L. Mazet, J.P. Germain, M. Bouvet, B. Malezieux, Thin Solid Films 490 (2005) 28.

14[14] M. Honda, K. Kanai, K. Komatsu, Y. Ouchi, H. Ishii, K. Seki, J. Appl. Phys. 102 (2007) 103704.

15[15] F. Haidu, A. Fechner, G. Salvan, O.D. Gordan, M. Fronk, D. Lehmann, B. Mahns, M. Knupfer, D.R.T. Zahn, AIP Advances 3 (2013) 062124.

16[16] L. Grządziel, M. Krzywiecki, Thin Solid Films 550 (2014) 361.

17[17] L. Grządziel, M. Krzywiecki, Mater. Chem. Phys. 149-150 (2015) 574.

18[18] C. Casiragi, S. Pisana, K.S. Novoselov, A.K. Geim, A.C. Ferrari, Appl. Phys. Lett. 91 (2007) 233108.

19[19] B.A. Kolesov, T.V. Basova, I.K. Igumenov, Thin Solid Films 304 (1997) 166.

20[20] M. Szybowicz, W. Bała, K. Fabisiak, K. Paprocki, M. Drozdowski, J. Mater. Sci. 46 (2011) 6589.

21[21] M. Szybowicz, J. Makowiecki, J. Mater. Sci. 47 (2012) 1522.

22[22] M.A. Shaibat, L.B. Casabianca, D.Y. Siberio-Perez, A.J. Matzger, Y. Ishii, J Phys Chem B. 114 (2010) 4400.

23[23] I. Horcas, R. Fernandez, J.M. Gomez-Rodriguez, J. Colchero, J. Gomez-Herrero and A. M. Baro, Rev. Sci. Instrum. 78 (2007) 013705.

24[24] M. Krzywiecki, L. Grządziel, J. Juszczyk, A. Kaźmierczak-Bałata, A. Erbe, J. Bodzenta, J. Phys. D: Appl. Phys. 47 (2014) 335304.

25[] J.R. Taylor, An Introduction to Error Analysis: The Study of Uncertainties in Physical Measurements University Science Books, Sausalito, 1997.

26[26] O. Berger, W.-J. Fischer, B. Adolphi, S. Tierbach, V. Melev, J. Schreiber, J. Mater. Sci. Mater. Electron. 11 (2000) 331.

27[27] M. Birkholtz, Thin Film Analysis by X-Ray Scattering, Wiley-VCH, Weinheim, 2006.

28[28] Z. Bao, A.J. Lovinger, A. Dodabalapur, Appl. Phys. Lett. 69 (1996) 3066.

29[29] M. Nakamura, Y. Morita, Y. Mori, A. Ishitani, H. Tokumoto, J. Vac. Sci. Technol. B 14 (1996) 1109.

30[30] H. Peisert, M. Knupfer, T. Schwieger, J.M. Auerhammer, M.S. Golden, J. Fink, J. Appl. Phys. 91 (2002) 4872.

31[31] F. Steinbach, H.H. Schmidt, J. Catal. 39 (1975) 190.

32[32] Y. Sadaoka, Y. Sakai, N. Yamazoe, T. Seiyama, Denki Kagaku 50 (1982) 457.

33[33] M. Krzywiecki, L. Grządziel, H. Peisert, I. Biswas, T. Chasse, J. Szuber, Thin Solid Films 518 (2010) 2688.

34[34] T. Szymański, M. Wośko, B. Paszkiewicz, R. Paszkiewicz, M. Drzik, J. Vac. Sci. Technol. A 33 (2015) 041506.

35[35] T.V. Basova, V.G. Kiselev, B.-E. Schuster, H. Peisert, T. Chasse, J. Raman Spectrosc. 40 (2009) 2080.

36[36] X. Wang, J. Zheng, K. Qiao, J. Qu, Ch. Cao, Appl. Surf. Sci. 297 (2014) 188.

37[37] G. Beaulieu-Houle, D.F.R. Gilson, I.S. Butler, Spectrochim. Acta A Mol. Biomol. Spectrosc. 117 (2014) 61.

38[38] G. Salvan, D. A. Tenne, A. Das, T.U. Kampen, D.R.T. Zahn, Org. Electron. 1 (2000) 49.

39[39] A. Guo, W. Li, X. Jiang, Ch. Wang, Y. Jiang, J. Raman Spectrosc. 46 (2015) 619.

40[40] O. Stenzel, A. Stendal, D. Drews, T. Werninghaus, M. Falke, D.R.T. Zahn, C. von Borczyskowski, Appl. Surf. Sci. 108 (1997) 71.

41[41] M.G. Torres, N.G. Fernandez, P.O. del Toro, M.R. Paneque, Nucleus 42 (2007) 41.

42[42] F. Paulat, T. Kuschel, Ch. Nalther, V.K.K. Praneeth, O. Sander, N. Lehnert, Inorg. Chem. 43 (2004) 6979.

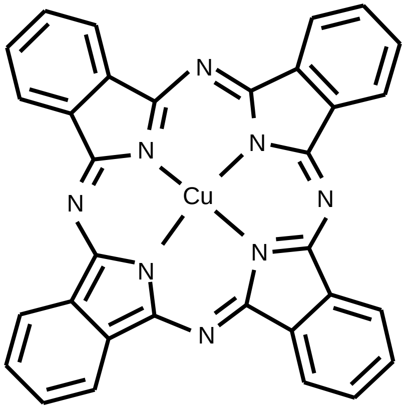
N
N
N
N
N
N
N
N
Cu

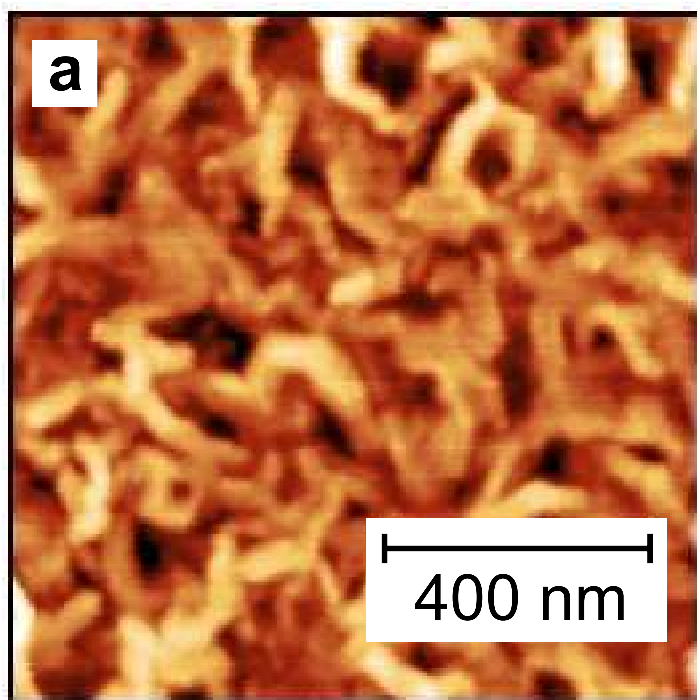
a
400 nm
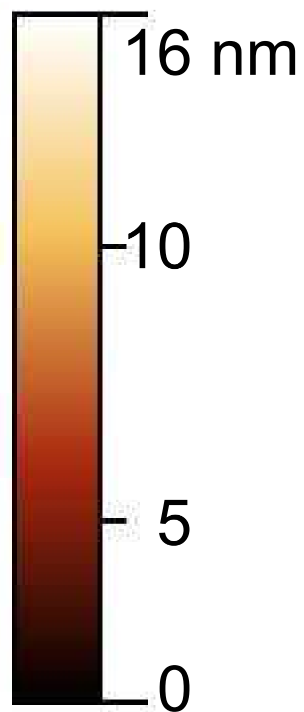
16 nm
10
5
0
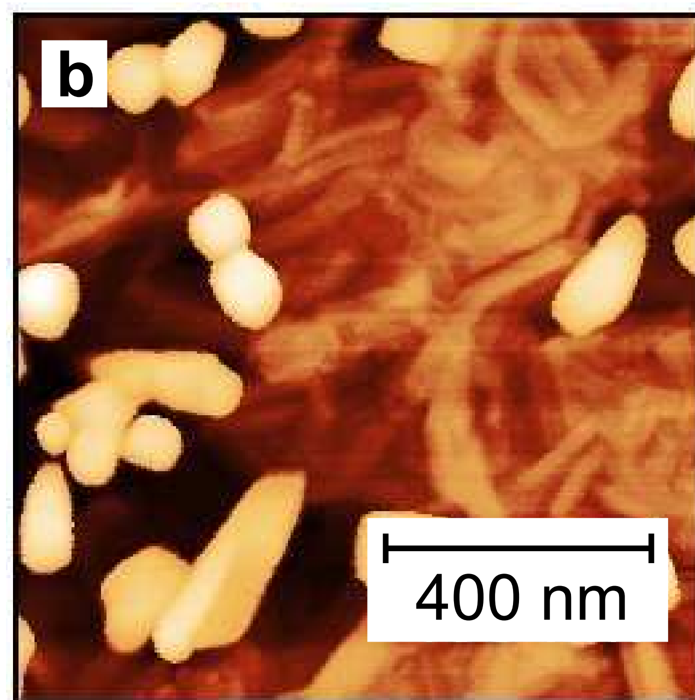
b
400 nm
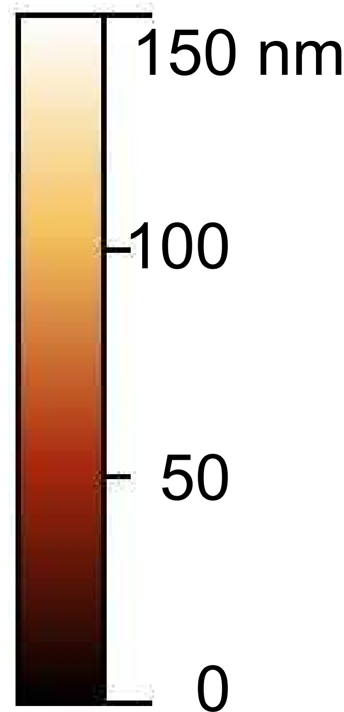
150 nm
100
50
0
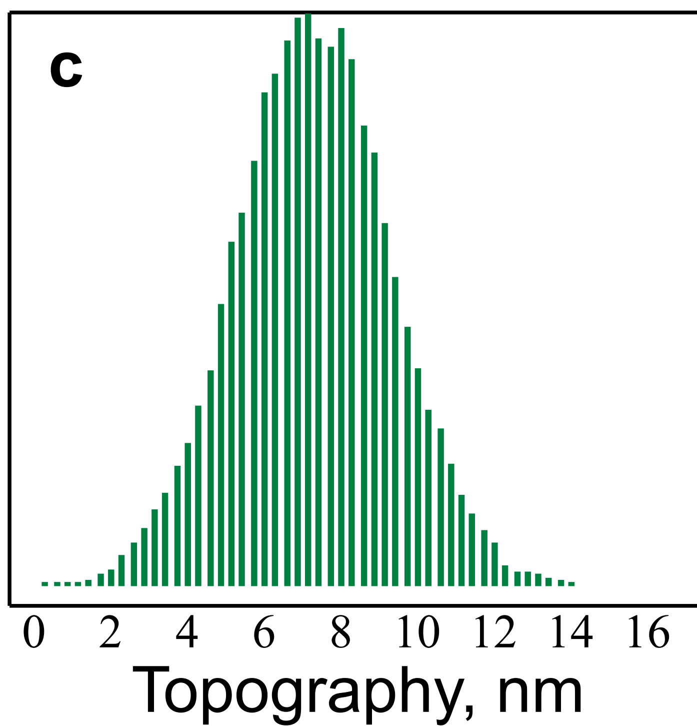
c
0 2 4 6 8 10 12 14 16
Topography, nm
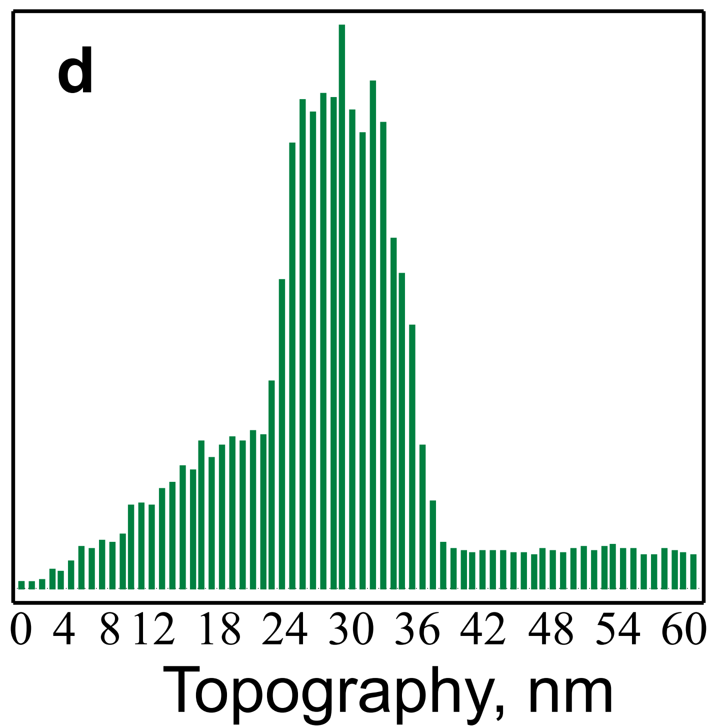
d
0 4 8 12 18 24 30 36 42 48 54 60
Topography, nm

a

100 nm

b

100 nm

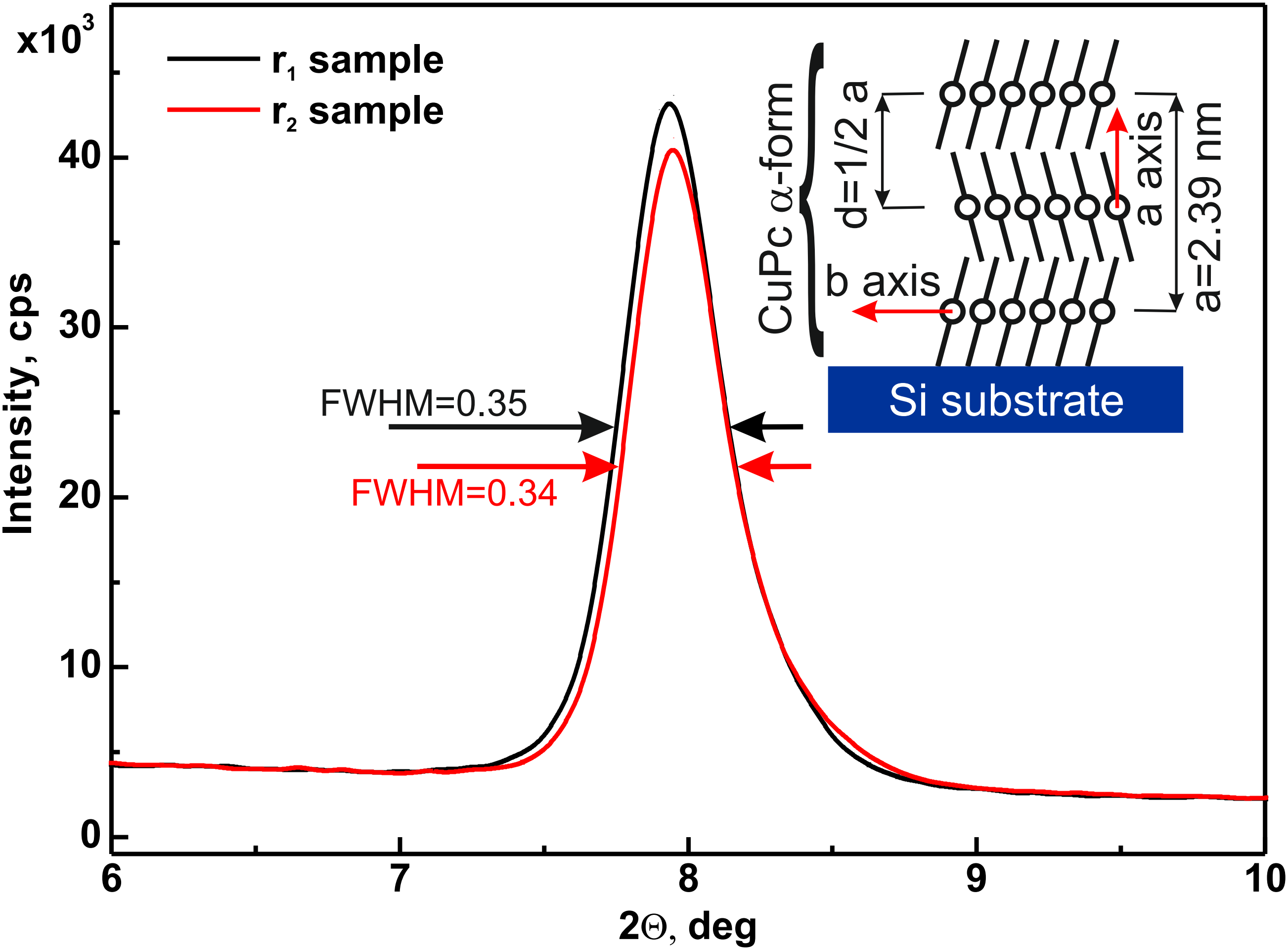

x10^3
r1 sample
r2 sample
CuPc α-form
d=1/2 a
a axis
a=2.39 nm
b axis
Si substrate
FWHM=0.35
FWHM=0.34
Intensity, cps
2Θ, deg
0
10
20
30
40
6
7
8
9
10

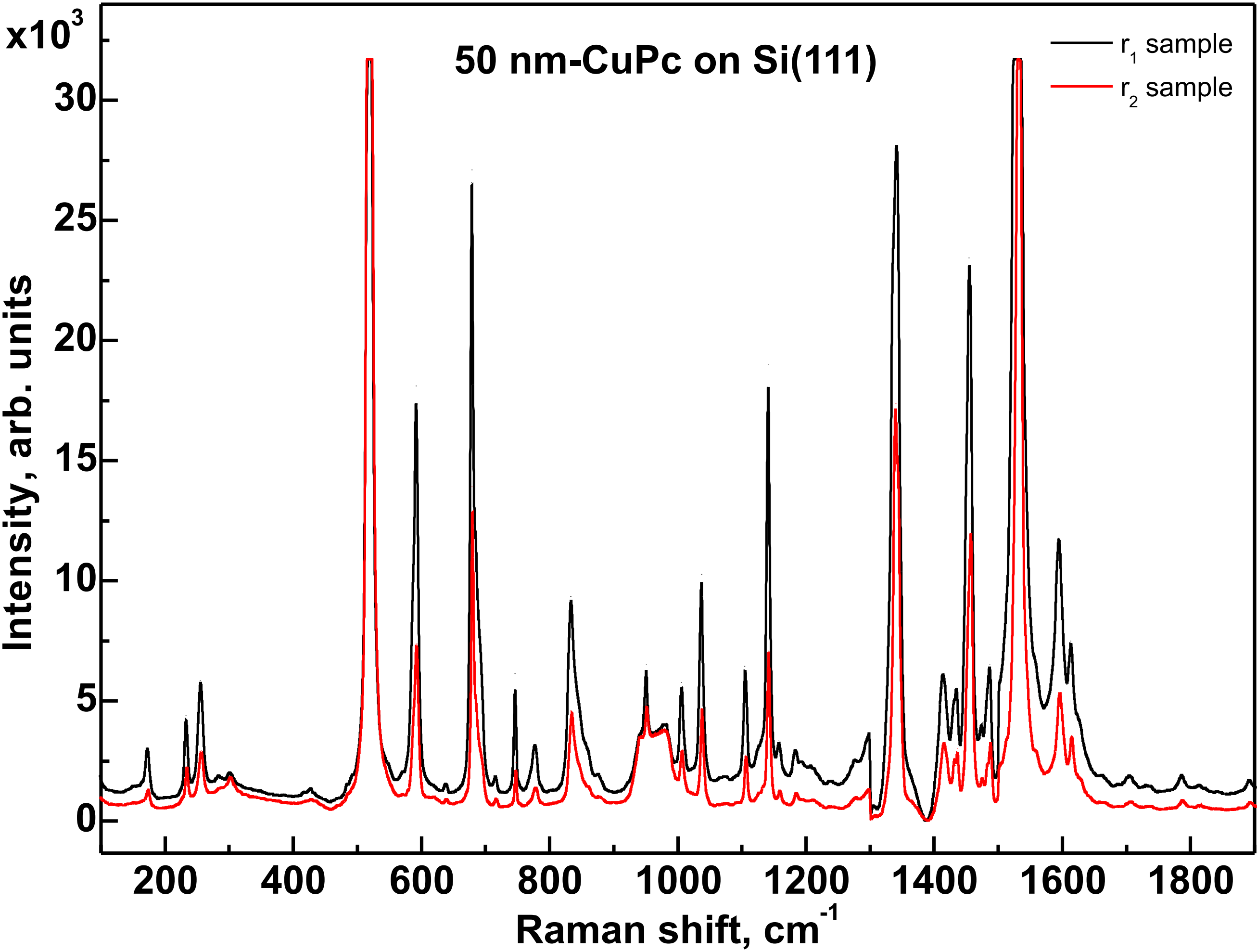

x10^3
50 nm-CuPc on Si(111)
r1 sample
r2 sample
Intensity, arb. units
Raman shift, cm-1
0
5
10
15
20
25
30
200
400
600
800
1000
1200
1400
1600
1800

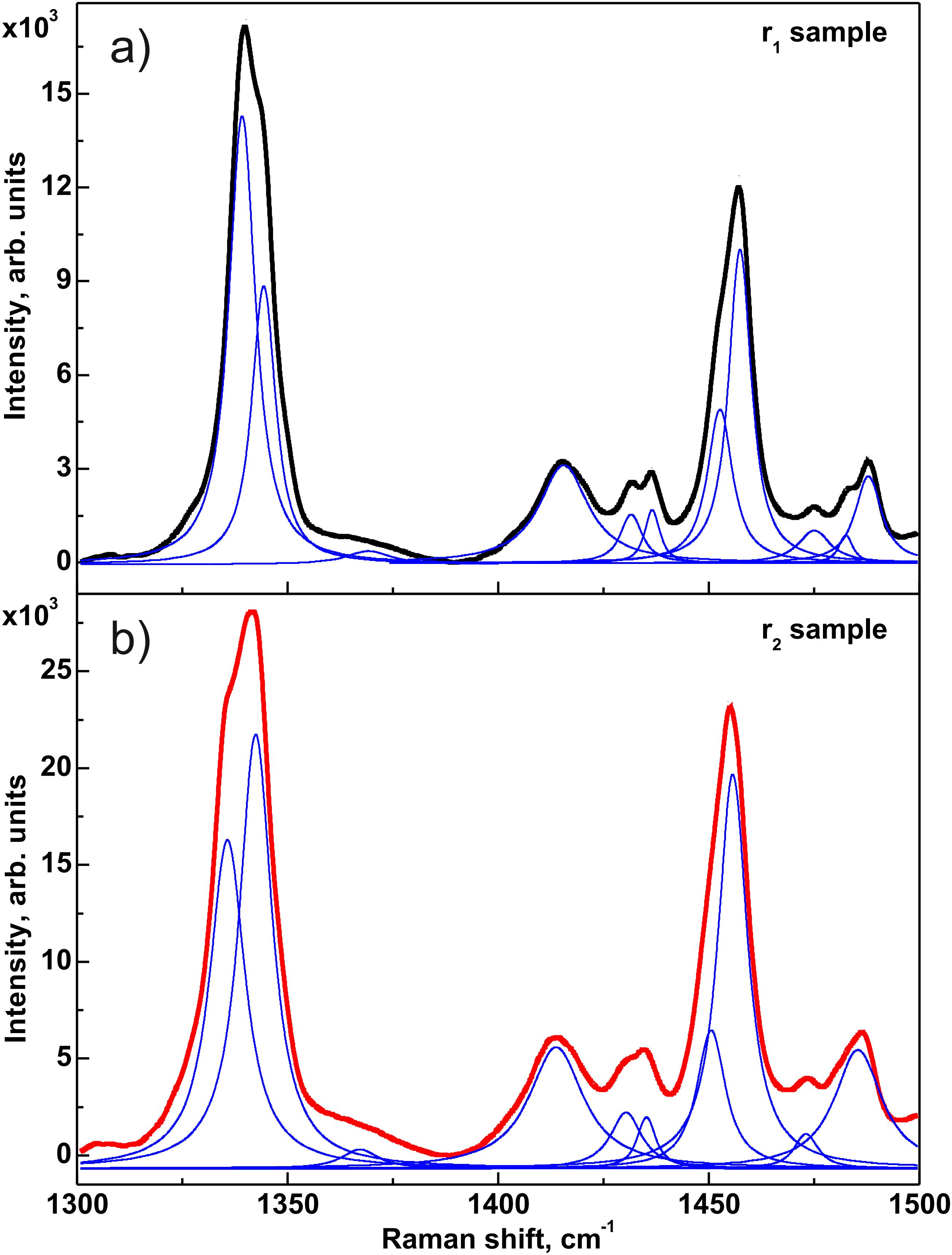

x10³
a)
r₁ sample
15
12
9
6
3
0
Intensity, arb. units
x10³
b)
r₂ sample
25
20
15
10
5
0
Intensity, arb. units
1300
1350
1400
1450
1500
Raman shift, cm⁻¹